Earth and Planetary Science Letters 394 (2014) 124–134

Contents lists available at ScienceDirect

Earth and Planetary Science Letters

www.elsevier.com/locate/epsl

The effect of total grain-size distribution on the dynamics of turbulent volcanic plumes

Frédéric Girault [a,b,*], Guillaume Carazzo [a], Steve Tait [a], Fabrizio Ferrucci [a,c], Édouard Kaminski [a]

[a] Institut de Physique du Globe de Paris, Sorbonne Paris Cité, Univ. Paris Diderot, CNRS, F-75005 Paris, France
[b] Laboratoire de Géologie, École Normale Supérieure, F-75005 Paris, France
[c] Department of Earth Science, Università della Calabria, Rende, Italy

ARTICLE INFO

Article history:
Received 27 November 2013
Received in revised form 4 March 2014
Accepted 11 March 2014
Available online xxxx
Editor: Y. Ricard

Keywords:
Plinian eruption
grain-size distribution
particle sedimentation
fragmentation
mass flux
airborne/satellite observation

ABSTRACT

The impact of explosive volcanic plumes on climate and on air traffic strongly depends on the concentration and grain-size distribution (GSD) of pyroclastic fragments injected into the atmosphere. Accurate and robust modelling of the evolution of GSD during pyroclast transport from the vent to the ash cloud is therefore crucial for the assessment of major volcanic hazards. Analysis of field deposits from various recent Plinian eruptions shows that their total GSD is well described by a power law, as expected from the physics of magma fragmentation, with an exponent (D) ranging from 3.0 to 3.9. By incorporating these measured GSD into the initial conditions of a steady-state 1D model of explosive eruption columns, we show that they have a first-order impact on the dynamical behaviour of explosive eruption columns. Starting from an initial value of D, the model tracks the evolution of GSD in the column and calculates the dynamical consequences of particle sedimentation. The maximum height reached by the column, one of the first-order results relevant to aircraft safety, changes by 30% for mass fluxes of 10^7 kg s^{-1} or larger, and by 45–85% for mass fluxes between 10^5 and 10^7 kg s^{-1}, depending on exponent D. We compare our predictions to a specially assembled set of geologic field data and remote sensing observations from 10 Plinian eruptions for which maximum column height and mass flux are known *independently*. The incorporation of realistic power-law GSD in the model greatly improves the predictions, which opens new perspectives for estimation of ash load and GSD in volcanic clouds from near real-time measurements available from satellite payloads. Our results also contribute to the improvement of volcanic source term characterization that is required input for meteorological dispersion models.

1. Introduction

Explosive volcanic eruptions inject large amounts of gas and pyroclast fragments into the atmosphere. The associated risks range from minor perturbations to total shutdown of air traffic (Miller and Casadevall, 2000), as well as from minor to major threats to humans (Hornwell, 2007) and ground infrastructure (Baxter et al., 2005), and finally perturbations to regional, hemispheric or global climate systems (Robock, 2000). Currently, a large research effort is taking place at the frontiers between the volcanology, meteorology and satellite remote sensing communities, whose overall purpose is to better understand the mode of ash injection into the atmosphere by explosive volcanic eruptions. This effort was in large part triggered by the Icelandic eruptions of Eyjafjallajökull (2010) and Grimsvötn (2011), and is continuing in the form of several international consortium projects, workshops and model benchmarking exercises whose instigators include official bodies such as those responsible for aviation safety, national and international space agencies.

Explosive eruptions are known to vary enormously in size (Sparks et al., 1997), measured either by their source mass fluxes or by the total amounts of material ejected, i.e. the integral of flux with respect to time. The over-riding demand of the meteorology and remote-sensing communities is for a substantially better quantification of the so-called “volcanic source term”, which means that researchers in volcanology should develop and validate methods enabling them to predict ash injection into the atmosphere in the vicinity of a volcano undergoing explosive eruption in terms of ash flux, concentration and grain-size distribution (GSD) of ash particles in a cloud, and finally height of injection. On the one hand, those developing algorithms for ash detection

* Corresponding author at: Laboratoire de Géologie, École Normale Supérieure, F-75005 Paris, France.
E-mail address: girault@biotite.ens.fr (F. Girault).

http://dx.doi.org/10.1016/j.epsl.2014.03.021
0012-821X/

from satellite measurements are faced with a non-unique inversion problem (e.g., Barsotti et al., 2008), meaning that the number of observables are less than the important variables, thus obliging them to make assumptions about some variables in order to obtain quantitative values for others. On the other hand, in order to carry out meaningful dispersion modelling and predict the vertical and horizontal distribution of ash in the atmosphere, meteorologists require input from volcanic source models as initial conditions (e.g., Slingo, 2010). As has been well known for decades from "routine" meteorological (weather prediction) modelling, the non-linear dynamics of the atmosphere requires that any model be given the most accurate initial conditions possible.

A number of physical processes which can interact with one another take place in volcanic eruption columns (Settle, 1978; Wilson et al., 1978; Sparks, 1986; Valentine and Wohletz, 1989; Woods and Bursik, 1991; Woods, 1993; Gilbert and Lane, 1994; Ernst et al., 1996; Glaze and Baloga, 1996; Glaze et al., 1997; Kaminski and Jaupart, 1998, 2001; Veitch and Woods, 2000; Bursik, 2001; Carazzo et al., 2008a; Ogden et al., 2008; Costa et al., 2010; Koyaguchi et al., 2010; Woodhouse et al., 2013; Degruyter and Bonadonna, 2013) and the potential complexity of physical models must be approached with care. In order to produce effective and robust results, these physical processes should be seen in a clear hierarchical sense, i.e. those that have leading order, second order etc. effects, in terms of their quantitative impact on results. Furthermore, it is crucial that such models are based on an appropriate representation of the mixture ejected from the volcanic vent, which should be consistent with the physical processes operating in the volcanic conduit below the ground surface. Leading order and secondary aspects should there also be carefully identified.

The starting point of the current paper, is a 1-dimensional dynamical model of a volcanic column, i.e. in which average column properties are calculated as a function of height consistent with a set of dynamical conservations laws (see details below), whose performance has been successfully tested against an extensive geological data-set (Carazzo et al., 2008b). The principal novelty of this model compared with others of similar basic architecture (Wilson, 1976; Sparks, 1986; Woods, 1988; Mastin, 2007; Kaminski et al., 2011) is that the entrainment parameter, describing quantitatively the key process of mixing rate of atmospheric air into the column, incorporates a dependence on local buoyancy which has in turn been validated against an extensive experimental data-set from the fluid dynamics literature (Kaminski et al., 2005; Carazzo et al., 2006, 2010). The first-order importance of the effect of variable entrainment parameter for volcanic columns arises from the fact that in order to rise high in the atmosphere, they must undergo a buoyancy inversion (from negative to positive), i.e. they start out as momentum jets whereas their upper parts are buoyant plumes. In the current work we further incorporate the effect of particle sedimentation from the side of the volcanic column (Fig. 1).

Sedimentation has already been shown to be potentially of first-order importance, by looking at plausible but schematic variations of grain-size (Woods and Bursik, 1991; Bursik et al., 1992; Ernst et al., 1996; Folch and Felpeto, 2005; Costa et al., 2006; Barsotti et al., 2008). Surprisingly, there has been no attempt to explore the quantitative effects on explosive columns of real volcanic GSD that have been measured by field studies. As we will show, enough such field data are now available to establish a reasonable mathematical description of total GSD. In the current work, we thus hope to contribute a set of robust first-order predictions regarding the injection of volcanic ash into the atmosphere due to a realistic set of eruption parameters with associated GSD. These predictions can be regarded as a volcanic source term, i.e. appropriate input for meteorological dispersion models.

2. Grain-size distribution in explosive volcanic eruptions

To study the evolution of the GSD in the eruptive column, from the vent to the umbrella, the initial step is to characterize the GSD at the vent. Several studies on fragmentation have shown that rocks fragment according to a power-law distribution (Hartmann, 1969; Turcotte, 1986; Alibidirov and Dingwell, 1996; Kaminski and Jaupart, 1998; Kueppers et al., 2006):

$$N(R \geqslant r) \propto r^{-D}, \tag{1}$$

where $N(R \geqslant r)$ is the number of particles with a radius larger than r, and D is the power-law exponent. Although log-normal and Gaussian laws are the most often used distributions in volcanology, only the power law is physically representative of the fragmentation process and is able to reproduce the GSD of various materials determined in the field and produced in laboratory experiments (Turcotte, 1986; Kueppers et al., 2006; Barnett et al., 2011; Pike et al., 2011; Haug et al., 2013).

The total GSD of an explosive eruption is not straightforward to determine: because the number of very large particles is generally rather low, significant uncertainty lies in sieving analyses for coarse grains (Koyaguchi and Ohno, 2001), and very fine particles tend to be transported over large distances from the volcanic vent and are easily lost. For example, recent analyses of fine ash particles of distal fallout deposits of the 1980 Mt. St. Helens, 1982 El Chichón and 1992 Mt. Spurr eruptions show that the amount of fine material can be significantly underestimated when working on proximal outcrops only (Rose et al., 2008; Rose and Durant, 2009; Durant and Rose, 2009). However, because fragmentation is a size-invariant process (Turcotte, 1986), the power law followed by the fragments can be determined using any (sufficiently large) range of sizes, in particular the sizes least likely to be affected by incorrect or incomplete sampling (Kaminski and Jaupart, 1998).

A review of total GSD available in the literature from various Plinian deposits emplaced during recent eruptions (Table 1) shows that power laws with exponents D ranging from 3.0 to 3.9 capture well the total GSD (Fig. 2). Uncertainties on the amount of large and fine particles are apparent in the curve fit, but they do not affect the determination of the power-law exponent, which is obtained with an uncertainty of ± 0.1. Gaussian laws, with means μ and standard deviations σ of the distributions, are also able to produce a good fit of the total GSD of these Plinian deposits (grey curves in Fig. 2). The differences between power and Gaussian laws lie first in the better ability of the Gaussian laws to account generally for the amounts of very fine ($>6\phi$, i.e. <15.6 μm) and very large particles ($<-3\phi$, i.e. >8 mm). However, due to the aforementioned large uncertainties, this difference between the power-law fit and the Gaussian law probably reflects the difference between the actual total GSD (power law) and the truncated GSD measured in the field (Gaussian law), as only power laws are based on a consistent physical description of magma fragmentation.

In explosive eruptions, the GSD, and hence the exact value of D, results from a combination of (primary) fragmentation in the conduit during rapid decompression of magma (e.g., Alibidirov and Dingwell, 1996), followed by preferential (secondary) re-fragmentation of larger fragments to produce fine ash higher in the conduit (Kaminski and Jaupart, 1998; Dufek et al., 2012). The exponent D is larger than 3 when the mass of the population of fragments resides primarily in fine ash particles, whereas values of D smaller than 3 reflect a dominant contribution of coarse particles to the total mass of the population. Because the amount of gas released by the magma forming a fragment depends on clast size (Kaminski and Jaupart, 1998), D controls in turn the total amount of gas released by the end of the fragmentation process, hence the amount of gas available in the volcanic mixture at the vent.

Table 1
Summary of the characteristics of the GSD available in the literature for the data-set of ten eruptions used for model validation. $\Delta\phi$ units correspond to the range of particle sizes studied in the field deposit (see reference). The determination of the power-law exponent D and of the Gaussian-law parameters (mean μ and standard deviation σ) is based on the reconstruction of the total GSD from field deposits (see Fig. 2).

Name of eruption	Atmospheric conditions	Altitude (km)	$\Delta\phi$ units	Power law D	Gaussian law $\mu \pm \sigma$	References
St. Vincent 1979	Tropical	1.234	−2/+8	3.0	2.7 ± 2.0	Brazier et al. (1982); Sparks and Wilson (1982); Kaminski and Jaupart (1998)
Fuego 1974a	Tropical	3.763	−5/+7	3.1	0.0 ± 1.6	Murrow et al. (1980); Rose et al. (2008)
Mt. Spurr Aug. 1992	Polar	3.374	−5/+10	3.1	3.0 ± 2.5	Durant and Rose (2009)
Mt. St. Helens 1980	Intermediate	2.549	−3/+10	3.1	5.0 ± 2.5	Carey and Sigurdsson (1982); Kaminski and Jaupart (2001)
Mt. Spurr Sept. 1992	Polar	3.374	−6/+10	3.2	4.0 ± 3.4	Durant and Rose (2009)
Nevado del Ruiz 1985	Tropical	5.321	−6/+4	3.2	3.0 ± 5.0	Kaminski and Jaupart (2001)
Ruapehu 1996	Intermediate	2.797	−7/+10	3.2	0.0 ± 2.5	Bonadonna and Houghton (2005)
El Chichón B 1982	Tropical	1.150	−4/+10	3.3	4.0 ± 2.5	Kaminski and Jaupart (2001); Rose and Durant (2009)
El Chichón C 1982	Tropical	1.150	−4/+10	3.3	4.0 ± 2.5	Kaminski and Jaupart (2001); Rose and Durant (2009)
Santa Maria 1902	Tropical	3.772	−5/+5	3.9	3.5 ± 2.7	Williams and Self (1983); Kaminski and Jaupart (1998)

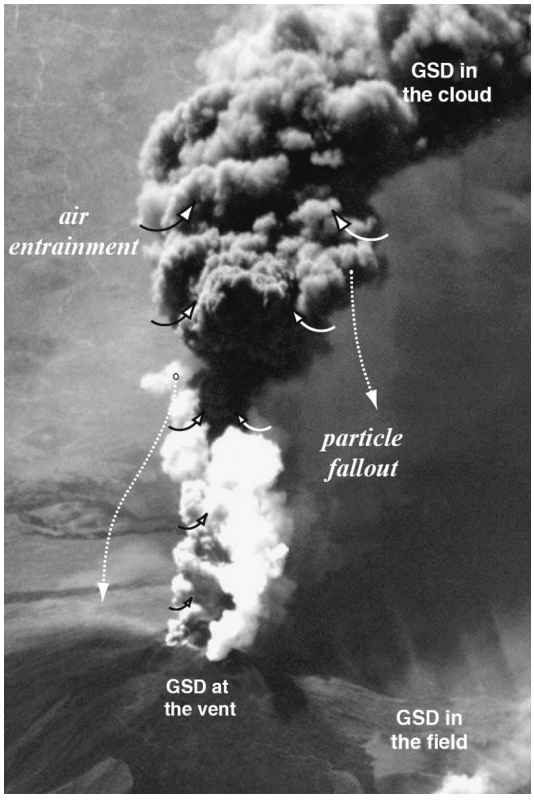

Fig. 1. Photograph of the Mt. Etna eruption on October 30th, 2002 illustrating the effects of air entrainment and particle sedimentation on the evolution of the grain-size distribution (GSD) from the volcanic vent to the umbrella cloud.

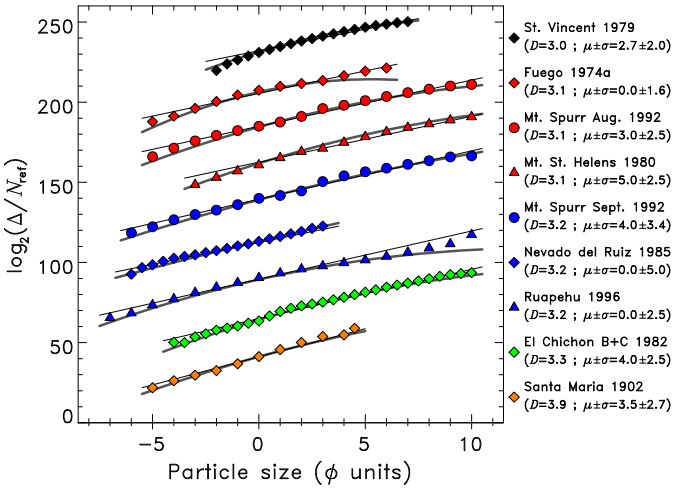

Fig. 2. Number of particles versus particle size for various Plinian deposits. The ϕ unit is related to the particle diameter d_ϕ by d_ϕ (mm) $= 2^{-\phi}$. Vertical axis corresponds to the logarithm to the base 2 of the number of fragments of each particle class Δ normalized by an arbitrary constant N_{ref} (Kaminski and Jaupart, 1998). The slope of each black line gives the value of the power-law exponent D at the vent. Grey curves correspond to Gaussian laws characterized by mean μ and standard deviation σ. The absolute uncertainty on D, determined by changing artificially the number of data points taken into account for the fits, is smaller than 0.1. Details on compiled data are available in Table 1.

D thus depends on the possible re-fragmentation processes in the conduit which themselves likely depend on the amount of gas released (Dufek et al., 2012). Complete modelling of fragmentation is beyond the scope of this paper and here we simply take D as an input parameter. The value of D thus exerts a major influence on source conditions (i.e. the total GSD and the amount of gas in the mixture) and hence, for given mass flux and total amount of gas dissolved in the magma, will also influence the dynamics of the volcanic plume (Kaminski and Jaupart, 2001) and the dispersion of pyroclasts in the atmosphere. We now show how the value of the power-law exponent can change the dynamics of the volcanic column when sedimentation is taken into account.

3. A physical model of explosive volcanic columns

The dynamics of explosive volcanic columns can be studied using various methods. 3D numerical methods have been developed based on average properties of the magmatic mixture (gas + pyroclasts) to study the systematic behaviour of plumes (e.g., Suzuki and Koyaguchi, 2012). Some 3D numerical methods considered the separated behaviour of the solid and the gas in the column, but because their numerical cost is large, they have been so far mainly used to study some specific volcanoes and/or eruptions (e.g., Ongaro et al., 2007). Here, we rely on the 1D steady-state "top-hat" approach which gives a useful average description of a turbulent eruption (Morton et al., 1956; Woods, 1988) and can easily include the evolution of the GSD from

the volcanic vent to the umbrella cloud due to sedimentation at the column margins in order to perform a systematic study.

3.1. Conservation and constitutive equations

The macroscopic conservation laws of mass, momentum, and energy fluxes in steady-state and for a particle-laden volcanic jet are written as, respectively (Bursik, 2001; Costa et al., 2006):

$$\frac{d}{dz}\left(\rho U R^2\right) = 2\rho_a U_e R + \sum_{\phi=1}^{N_\phi} \frac{dQ_\phi}{dz}, \tag{2}$$

$$\frac{d}{dz}\left(\rho U^2 R^2\right) = g(\rho_a - \rho)R^2 + U\sum_{\phi=1}^{N_\phi} \frac{dQ_\phi}{dz}, \tag{3}$$

$$\frac{d}{dz}\left(\rho c_p T U R^2\right) = 2\rho_a U_e R c_a T_a - \rho_a g U R^2 + c_p T \sum_{\phi=1}^{N_\phi} \frac{dQ_\phi}{dz}, \tag{4}$$

where $R(z)$ is the column radius, $U(z)$ is the average ascent velocity, g is the acceleration of gravity, Q_ϕ is the flux of ϕ-sized particles ($\mathrm{kg\,s^{-1}}$) (distributed within 20 classes of grain sizes ranging from 10ϕ (1 μm) to -9ϕ (0.5 m) with one ϕ intervals), c_a, T_a and ρ_a are the specific heat, temperature and density of the atmosphere, respectively, and c_p, T and ρ are those of the bulk mixture. U_e is the entrainment rate at the edge of the plume, defined as $U_e = \alpha_e U$, where α_e is the top-hat entrainment coefficient of Morton et al. (1956). We consider here that the rate of entrainment depends on the buoyancy of the column relative to the ambient air and can be expressed as (Kaminski et al., 2005):

$$\alpha_e = \frac{C}{2} + \left(1 - \frac{1}{A}\right)\mathrm{Ri}, \tag{5}$$

where $\mathrm{Ri} = g(\rho_a - \rho)R/\rho_a U^2$ is the local Richardson number in the plume, and C and A are dimensionless parameters that depend on the flow structure and have been constrained in previous studies (Carazzo et al., 2006, 2008a). At that stage, we do not consider thermal or mechanical disequilibrium between the volcanic gas and the particles, which are important for large fragments (Woods and Bursik, 1991). This limitation is likely to be of little importance as large particles, as shown below, will be lost by sedimentation relatively early as the column rises.

The set of conservation equations is complemented by constitutive equations for the evolution of the thermodynamic properties of the column with altitude (Woods, 1988):

$$\frac{1}{\rho} = \frac{(1 - x_g)}{\rho_p} + \frac{x_g R_g T}{P_a}, \tag{6}$$

$$R_g = R_a + (R_{g_0} - R_a)\left(\frac{1 - x_g}{x_g}\right)\left(\frac{x_{g_0}}{1 - x_{g_0}}\right), \tag{7}$$

$$c_p = c_a + (c_{p_0} - c_a)\left(\frac{1 - x_g}{1 - x_{g_0}}\right), \tag{8}$$

where $x_g(z)$ is the gas mass fraction, $P_a(z)$ is the atmospheric pressure, $R_{g_0} = 461\ \mathrm{J\,kg^{-1}\,K^{-1}}$ and $R_a = 287\ \mathrm{J\,kg^{-1}\,K^{-1}}$ are the bulk column and the air gas constants, respectively. The subscript 0 refers to initial values of the variables at the vent. The atmospheric conditions are taken as typical polar, intermediate and tropical conditions using the same parameterization as in Glaze and Baloga (1996).

3.2. Particle fallout

As in previous studies (Woods and Bursik, 1991; Ernst et al., 1996), the mass loss of ϕ-sized particles from the edges of the column is assumed to be proportional to the mass flux of particles, Q_ϕ, and to the terminal fall velocity corresponding to the size of particles, V_ϕ, such as:

$$\frac{dQ_\phi}{dz} = -p_s \frac{Q_\phi}{R}\frac{V_\phi}{U}, \tag{9}$$

where p_s is a probability of sedimentation taken equal to 0.27 ± 0.01 as in Ernst et al. (1996). For a given particle size, the fallout velocity, V_ϕ, is calculated using the formulae of Bonadonna et al. (1998):

$$V_\phi = \begin{cases} \sqrt{\dfrac{3.1 d_\phi g(\rho_p - \rho)}{\rho_a}} & \text{for } \mathrm{Re}_\phi \geqslant 500, \\ d_\phi\left(\dfrac{4g^2(\rho_p - \rho)^2}{225\mu\rho_a}\right)^{1/3} & \text{for } 0.4 \leqslant \mathrm{Re}_\phi \leqslant 500, \\ \dfrac{d_\phi^2 g(\rho_p - \rho)}{18\mu} & \text{for } \mathrm{Re}_\phi \leqslant 0.4, \end{cases} \tag{10}$$

which depends on the Reynolds number of the particles, $\mathrm{Re}_\phi = d_\phi V_\phi \rho/\mu$, where d_ϕ is the particle diameter of clast ϕ, $\mu(z)$ is the dynamic viscosity of air and $\rho_p = 2000\ \mathrm{kg\,m^{-3}}$ is the particle density.

The set of conservation equations (Eqs. (2)–(4)), without the sedimentation terms (i.e. $dQ_\phi/dz = 0$), have been used in the vast majority of Plinian eruption studies based on the 'dusty gas hypothesis' (e.g., Woods, 1988; Sparks et al., 1997; Mastin, 2007; Kaminski et al., 2011; Burden et al., 2011). Alternative models incorporate the sedimentation terms in Eqs. (2)–(4) (Folch and Felpeto, 2005; Pfeiffer et al., 2005; Costa et al., 2006; Barsotti et al., 2008), but they do not systematically study the potential effect of the GSD on the plume dynamics. Here, to reach this goal, we use power-law GSD consistent with field observations.

3.3. Exit conditions at the volcanic vent

The eruptive mass flux is the main parameter controlling the height reached by the volcanic plume and the rate of ash injection in the atmosphere (e.g., Wilson et al., 1978; Woods, 1988; Sparks et al., 1997). We consider here mass fluxes ranging from 10^5 to $10^9\ \mathrm{kg\,s^{-1}}$, which correspond to the range of intensity of common explosive eruptions (from sub-Plinian to ultra-Plinian). The second important parameter is the amount of gas in the volcanic mixture, x_{g_0}, through its control on the jet velocity at the vent, U_0. In the following, we will use the hypothesis of a choked jet at the vent according to which U_0 is given by (Woods and Bower, 1995):

$$U_0 = 1.8\sqrt{x_{g_0} R_{g_0} T_0}, \tag{11}$$

where T_0 is the magma temperature. For the sake of the argument, we will take the average temperature of andesitic magma ($T_0 = 1200$ K) and a fraction of gas of 4 wt%. We make this choice of using one single temperature and one single gas content to focus on the influence of GSD, and discussion on the implication of these hypotheses can be found in previous studies (e.g., Carazzo et al., 2008b; Koyaguchi et al., 2010). In the following we will use the power-law exponent together with the results of Kaminski and Jaupart (1998) to set x_{g_0} at the vent. Under these conditions and considering a choked plume (which yields $130 \leqslant U_0 \leqslant 270\ \mathrm{m\,s^{-1}}$ in the range of cases we consider), all 20 classes of grain sizes ranging from 10ϕ (1 μm) to -9ϕ (0.5 m) are entrained in the ascending column because fall velocity of all particle sizes is smaller than U_0.

In summary, the model applies when the population of fragments is dominated by ash particles, which is commonly the case during explosive eruptions, and when there is no strong overpressure at the base of the column. This latter condition is usually

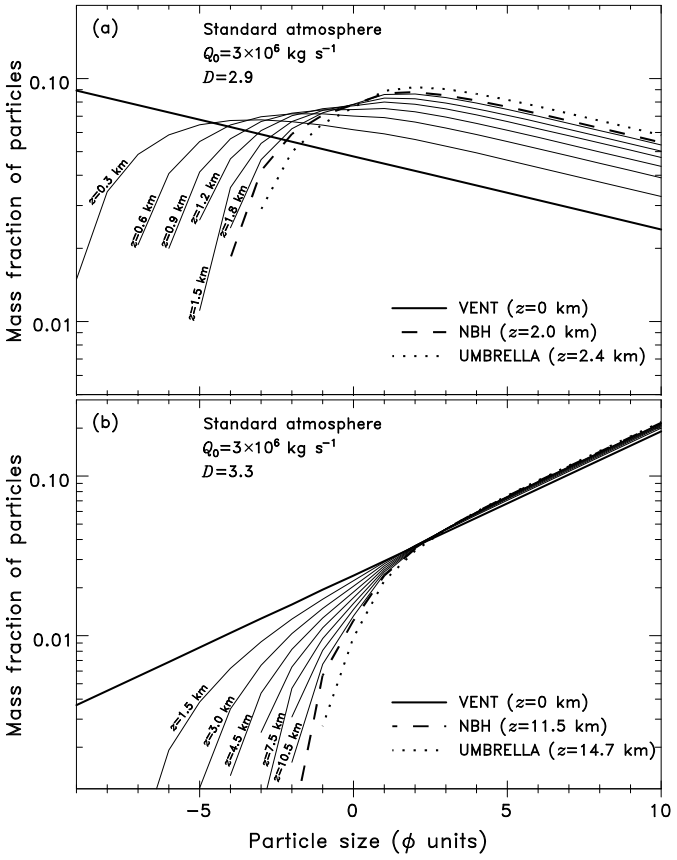

Fig. 3. Predictions of the evolution of the GSD from the vent to the maximum height of the eruptive column for two values of the power-law exponent: (a) $D = 2.9$ and (b) $D = 3.3$. The ϕ unit is related to the particle diameter d_ϕ by d_ϕ (mm) $= 2^{-\phi}$. NBH corresponds to the neutral buoyancy height of the eruptive column.

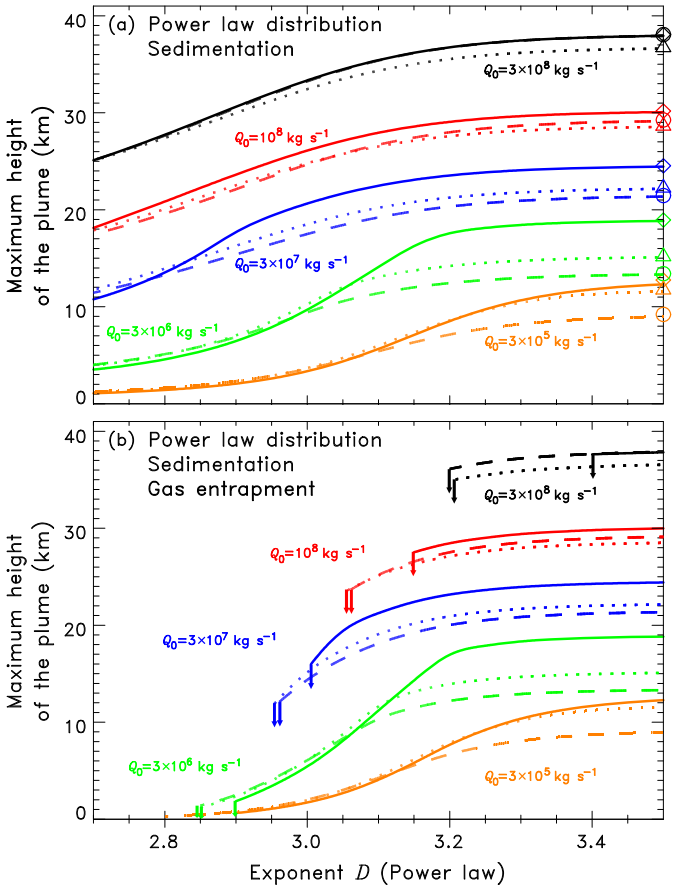

Fig. 4. Theoretical predictions of the maximum height reached by a volcanic column as a function of the power-law exponent D for different atmospheric conditions and source mass fluxes. In (a), the modelling takes into account a power-law GSD with particle sedimentation. Symbols at large D value correspond to the predictions in the case of the dusty gas hypothesis (no sedimentation). In (b), the modelling takes into account a power-law GSD with particle sedimentation and gas entrapment. Vertical arrows show the collapse of the plume. Solid, dashed and dotted curves correspond to predictions made for tropical, polar and intermediate atmosphere, respectively.

met at the vent for small explosive eruptions, and within a few hundred meters above the vent for large explosive eruptions (see Carazzo et al. (2008b) or Suzuki and Koyaguchi (2012) for a detailed discussion of these assumptions).

4. Results of the model

The set of equations is solved using a fourth-order Runge–Kutta algorithm with an altitude step size of 1 m. The results of the model are the evolution of the GSD in the column as a function of height, and the steady-state maximum column height attained as a function of the mass flux and of the power-law exponent.

The GSD imposed at the vent evolves as the mixture rises to its maximum height, depending on the initial value of the power-law exponent D. Two examples of the tracking of GSD in the eruptive column are shown in Fig. 3 for a given mass flux at the vent and standard atmospheric conditions. When the GSD is initially dominated by coarse particles ($D < 3$; Fig. 3a), a large amount of coarse material is quite rapidly lost by sedimentation, which leads to a significant decrease of median particle size in the eruptive column as it rises. Conversely, when the GSD is initially dominated by fine particles ($D > 3$; Fig. 3b), the mass of particles in the column remains relatively constant with altitude because fine particles do not fallout significantly during the ascent of the plume. In other words, large particles are always affected by sedimentation, but their contribution to the total mass of particles is negligible when $D > 3$, hence the effect of sedimentation is also quite small in that case. Because the mass flux in the column is controlled by the mass flux of particles, sedimentation of large clasts for $D < 3$ will reduce the total mass flux in the column. This will tend to reduce the maximum height of the plume because large particles lost from the column do not transfer their thermal energy to the entrained ambient air.

The effect of the power-law exponent on the maximum height reached by a volcanic plume has been studied systematically. We found first that the maximum height reached by a volcanic column is mainly controlled by the mass flux at the source and, to a lesser extent, by the stratification of the atmosphere (Fig. 4), which is consistent with previous studies (e.g., Wilson et al., 1978; Woods, 1988; Sparks et al., 1997; Mastin, 2007; Carazzo et al., 2008a; Woodhouse et al., 2013; Degruyter and Bonadonna, 2013). A new result is the effect of the value of D on the maximum height reached by the column. While the dusty gas hypothesis yields a single value of the maximum column height (symbols in Fig. 4a), the effect of sedimentation considerably changes the maximum height when $D < 3.3$. For relatively low and intermediate mass fluxes ($10^5 \leqslant Q_0 \leqslant 3 \times 10^7$ kg s^{-1}), the maximum height can vary by an order of magnitude for a given mass flux depending on the value of D (Fig. 4a). Columns enriched in large particles (i.e., with $D < 3$) are more sensitive to this effect than columns enriched in fine particles (i.e., with $D > 3$) as fine particles are not significantly lost by sedimentation. For higher mass fluxes ($Q_0 > 3 \times 10^7$ kg s^{-1}), the maximum height becomes relatively insensitive (variation $\leqslant$15%) to the value of D at the vent if the column is enriched in fine particles ($D > 3$), but the maximum

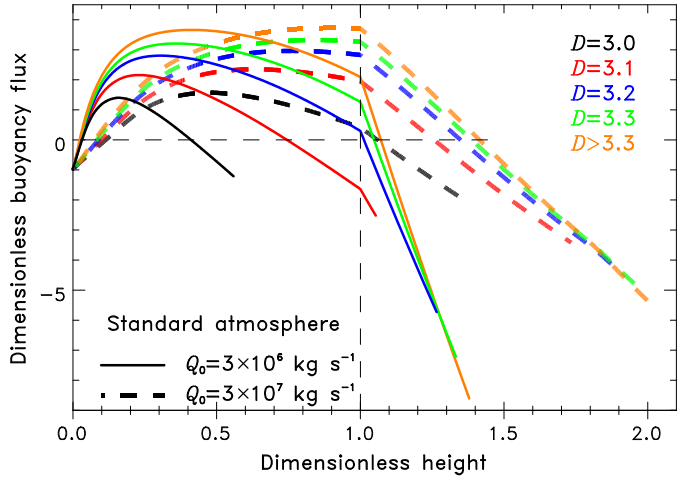

Fig. 5. Dimensionless buoyancy flux per unit mass (normalized by the absolute buoyancy flux at the vent) as a function of dimensionless height (normalized by the altitude of the tropopause) for different power-law exponents D and two eruptive mass fluxes at the vent.

height can still decrease by almost 10 km if the value of D is smaller than 2.8. For a given mass flux, no significant change is observed once D has reached a value larger than 3.3; the rate of sedimentation is then low enough to be close to the dusty gas limit.

When gas entrapment in pumices is taken into account (Fig. 4b), a new phenomenon occurs, i.e., column collapse. This happens when the mass flux at the vent is too large relative to the momentum flux to be carried up to the height of buoyancy inversion. Because the ratio of the two fluxes is simply the eruptive velocity at the vent, which itself is a function of the gas present in the mixture, it will decrease for a decreasing value of D (Kaminski and Jaupart, 2001). For each mass flux, there is a threshold value of D for which the amount of gas, hence the velocity at the vent, is not large enough to attain the buoyancy inversion. In this case of column collapse, no maximum height is reported in Fig. 4b.

The evolution with altitude of the buoyancy flux of the plume also illustrates the effect of the sedimentation on the volcanic column (Fig. 5). In the case where sedimentation is negligible ($D > 3.3$) the buoyancy flux first increases by heating of the engulfed air and then starts to decrease (due to density stratification of the atmosphere) as the column rises in the atmosphere. If the column reaches the tropopause, the decrease becomes faster and larger as the stratosphere is much less dense than the column. When sedimentation is effective ($D \leqslant 3.3$), the initial increase of the buoyancy flux is reduced because the coarse particles, that represent the thermal reservoir of the mixture, are lost by sedimentation. For the same reason, the decrease of the buoyancy flux in the upper part of the atmosphere is enhanced for coarser GSD.

Our results show that the GSD in explosive volcanic columns has a major influence on the plume rise if the exponent of the power-law GSD is $\leqslant 3.3$: the maximum height is reduced by ca. 30% for mass fluxes of 10^7 kg s^{-1} or larger, and up to 45–85% for mass fluxes between 10^5 and 10^7 kg s^{-1}. This value of D defines a threshold below which the flow is no longer well described by the 'dusty gas hypothesis'. For values of D smaller than 3.3, the amount of exsolved gas at the base of the column can be significantly reduced due to gas entrapment in large particles. In addition, large particles will settle rapidly from the edges of the column, which will reduce the amount of thermal energy available to heat the entrained atmospheric air and to increase buoyancy in the column. The combination of these two effects contributes to lower the maximum height reached by the column, and will eventually produce column collapse if the mass flux is large enough.

5. Discussion

We have shown that the GSD can have a first-order influence on the maximum height reached by a volcanic column. Now, it is worthwhile, first, to test the model presented above by comparing the calculations with data, second, to investigate the implications of the model for the rate of ash injection into the atmosphere and, third, to discuss the associated effects of wind and GSD on the maximum height.

5.1. Model validation

To validate our theoretical model and the obtained impact of GSD on plume dynamics, we compared its predictions with natural cases. For this, we assembled data from a series of recent eruptions by seeking those for which the source conditions and the maximum column height were determined *independently* (i.e. the eruptive mass flux is not determined from the column height) and for which the total GSD was also available. We were able to find 10 eruptions (Table 2) for which the total GSD is constrained from the field deposits (Table 1), the average mass flux is determined from the eruption volume and duration, and the column height is measured either by a visual observation from the ground or on airplanes, by isopleth maps built from the distribution of the deposits, or by satellite-, airplane-, or ground-based radar measurements. The predicted and measured eruptive mass fluxes are compared for these 10 eruptions based on the maximum height reached by the eruptive column. For each event, predicted mass flux is assessed to match the reported maximum height of the column and its uncertainty is estimated in order to account for a one-sigma standard deviation around the mean value of the maximum height reached by the column (Table 2).

In a first stage (Fig. 6a), we use the classical 'dusty gas hypothesis' as defined above (no sedimentation). Discrepancies between predicted and measured mass fluxes are considerable for all cases except El Chichón C (1982) and Santa Maria (1902), and are more important for small mass fluxes. The dusty gas hypothesis therefore does not reproduce the independent data-set, in particular for mass fluxes smaller than 4×10^7 kg s^{-1}.

In a second stage (Fig. 6b), we use the power-law GSD at the vent (see Fig. 2 and Table 1 for values of D) and include particle sedimentation. The predicted mass fluxes are still lower than those measured in all cases, but are closer to the data than those predicted using the dusty gas hypothesis. In particular, the mass fluxes of the Aug. 1992 Mt. Spurr, 1980 Mt. St. Helens and 1902 Santa Maria eruptions are better predicted in this second case.

In a third stage (Fig. 6c), we use the power-law GSD at the vent and include the effects of particle sedimentation and gas entrapment in large pumices. These three ingredients yield a better prediction than in the two previous stages. The best match with data is obtained for mass fluxes of the 1974a Fuego, 1980 Mt. St. Helens, 1996 Ruapehu, Aug. 1992 Mt. Spurr and 1979 St. Vincent eruptions, whereas the fluxes predicted for the eruptions of Mt. Spurr (Sept. 1992) and El Chichón (B + C, 1982) are still a bit low.

As a fourth stage (Fig. 6d), we use a Gaussian-law GSD at the vent (see Fig. 2 and Table 1 for values of μ and σ) and include the effects of particle sedimentation and gas entrapment in large pumices. The resulting mass fluxes of all the 10 eruptions are better predicted than with the dusty gas hypothesis, but the difference between measured and observed mass fluxes is significantly larger than for a power-law GSD. This result is due both to the larger sensitivity of the power-law GSD to the sedimentation process and to the underestimation of the amount of the smallest particles in the Gaussian-law GSD compared with the power-law. This quantitative test, therefore, demonstrates that "real" GSD is an

Table 2
Summary of the measured eruptive mass flux and maximum height determined *independently* and available in the literature for the data-set of ten eruptions used for model validation. Methods used to estimate the maximum height are: (v) visual observation from the ground or on airplanes, (i) isopleth maps, and (r) satellite-, airplane-, or ground-based radar measurements. The volume DRE is the dense-rock equivalent of the erupted volume. Uncertainties on mass flux and maximum height correspond to the standard deviation of the respective independent values available in the literature for a given eruption.

Name of eruption	Atmospheric conditions	Altitude (km)	Volume DRE (km^3)	Duration (h)	Mass flux ($kg\,s^{-1}$)	Maximum height above vent (km)	References
St. Vincent 1979	Tropical	1.234	0.14	2.5–3.5	$(3.4 \pm 0.6) \times 10^7$	16 ± 3 (v)	Anderson and Flett (1903); Carey and Sigurdsson (1978); Mastin et al. (2009)
Fuego 1974a	Tropical	3.763	0.02	5	$(3.0 \pm 0.9) \times 10^6$	10 ± 1 (v)	Murrow et al. (1980); Mastin et al. (2009)
Mt. Spurr Aug. 1992	Polar	3.374	0.014	3.5	$(3.0 \pm 0.9) \times 10^6$	10.5 ± 1.0 (r)	Neal et al. (1995); Eichelberger et al. (1995); McGimsey et al. (2001); Mastin et al. (2009)
Mt. St. Helens 1980	Intermediate	2.549	0.24	9.1	$(1.6 \pm 0.4) \times 10^7$	17.5 ± 0.5 (r)	Sarna-Wojcicki et al. (1981); Carey and Sigurdsson (1989); Carey et al. (1990); Durant et al. (2009)
Mt. Spurr Sept. 1992	Polar	3.374	0.015	3.6	$(3.0 \pm 0.9) \times 10^6$	10.7 ± 1.0 (r)	Neal et al. (1995); Eichelberger et al. (1995); McGimsey et al. (2001); Mastin et al. (2009)
Nevado del Ruiz 1985	Tropical	5.321	0.014–0.039	0.33	$(4.0 \pm 1.4) \times 10^7$	26.5 ± 3.0 (i)	Naranjo et al. (1986); Carey and Sigurdsson (1989); Carazzo et al. (2008b); Mastin et al. (2009)
Ruapehu 1996	Intermediate	2.797	0.002	6.5	$(2.0 \pm 0.6) \times 10^5$	5.7 ± 0.6 (r)	Prata and Grant (2001); Mastin et al. (2009)
El Chichón B 1982	Tropical	1.150	0.4	1.8	$(1.1 \pm 0.6) \times 10^8$	24 ± 2 (i)	Carey and Sigurdsson (1986, 1989)
El Chichón C 1982	Tropical	1.150	0.4	3.3	$(6.3 \pm 3.2) \times 10^7$	22 ± 2 (i)	Carey and Sigurdsson (1986, 1989); Carazzo et al. (2008b)
Santa Maria 1902	Tropical	3.772	3.3–8.6	24–36	$(8.8 \pm 5.6) \times 10^7$	31 ± 4 (i)	Anderson (1908); Rose (1972); Carey and Sparks (1986); Carey and Sigurdsson (1989); Carazzo et al. (2008b); Mastin et al. (2009)

essential ingredient to be included in theoretical models to provide a robust prediction of the mass flux of Plinian eruptions.

5.2. Rate of ash injection into the atmosphere

One of the key predictions of the model for risk assessment is the amount of ash particles injected into the atmosphere (Bonadonna et al., 2012; Prata and Prata, 2012). The fraction of fine particles predicted by the model at the top of the column is shown in Fig. 7a as a function of the maximum height of the column (corresponding to different eruptive mass fluxes, e.g., Fig. 4) for different power-law GSD at the vent. Fine particles correspond here to sizes smaller than or equal to 15.6 μm (6ϕ). When the population of pyroclasts contains mainly fine ash particles (i.e., $D > 3.3$), the amount of fine particles remains relatively constant whatever the altitude reached by the volcanic plume. By contrast, for lower values of D (i.e., $D \leqslant 3.3$), the fraction of fine particles decreases as the plume rises due to sedimentation. This decrease is more important above 10–20 km, an altitude range corresponding to the height of the tropopause, depending on the atmospheric conditions. At this altitude, the atmospheric density changes sharply, which decreases the average velocity of the plume (Glaze and Baloga, 1996), hence increases particle sedimentation.

Calculations of the rate of ash injection (Q_ϕ^{ash}) are illustrated in Fig. 7b as a function of the maximum height (H) of the eruptive column for different power-law GSD at the vent. For heights smaller than 10 km, the rate of ash injection decreases as D increases. In the case of a small D value and large particle sedimentation, larger mass fluxes at the vent are required in order for the plume to reach a given height. The increase of the rate of ash injection with the maximum height of the column can be separately fitted for tropospheric and stratospheric heights using a power-law relationship $(Q_\phi^{\mathrm{ash}}/Q_{\mathrm{ref}}) = a(H/H_{\mathrm{ref}})^b$, similar to the scaling law that gives the maximum height of a plume (e.g., Morton et al., 1956; Briggs, 1969; Woods, 1988), where $H_{\mathrm{ref}} = 36.4$ km is the mean maximum height obtained for $Q_{\mathrm{ref}} = 10^8$ $kg\,s^{-1}$ at the vent. For column heights greater than 15 km, i.e. stratospheric heights, only small differences in the rate of ash injection are observed as a function of D and average parameters ($a = 2.23$, $b = 5.06$) can be used. For column heights lower than 15 km, i.e. in the troposphere, the GSD can change the rate of ash injection by over one order of magnitude for a given column height and the fitting parameters range between ($a = 0.38$, $b = 2.11$) for $D = 3.0$ to ($a = 0.37$, $b = 4.01$) for $D > 3.3$. Although the rate of ash injection is positively correlated with height (i.e., with the eruptive mass flux), ash concentration in the plume can be anti-correlated with height because of reduced entrainment. This is explained by the fact that, when the eruptive mass flux is large, the buoyancy flux remains negative over a greater range of height (see Fig. 5), which reduces the entrainment of atmospheric air (Eq. (5) shows how negative Richardson number reduces α_e). The effect of D becomes especially critical near the tropopause, i.e., between 9 and 17 km high depending on the atmospheric conditions (Fig. 7b), because of the decrease of the average velocity of the plume. This threshold altitude confirms therefore the significant effect of the tropopause on volcanic plume dynamics for risk assessment in relation to civil aircraft.

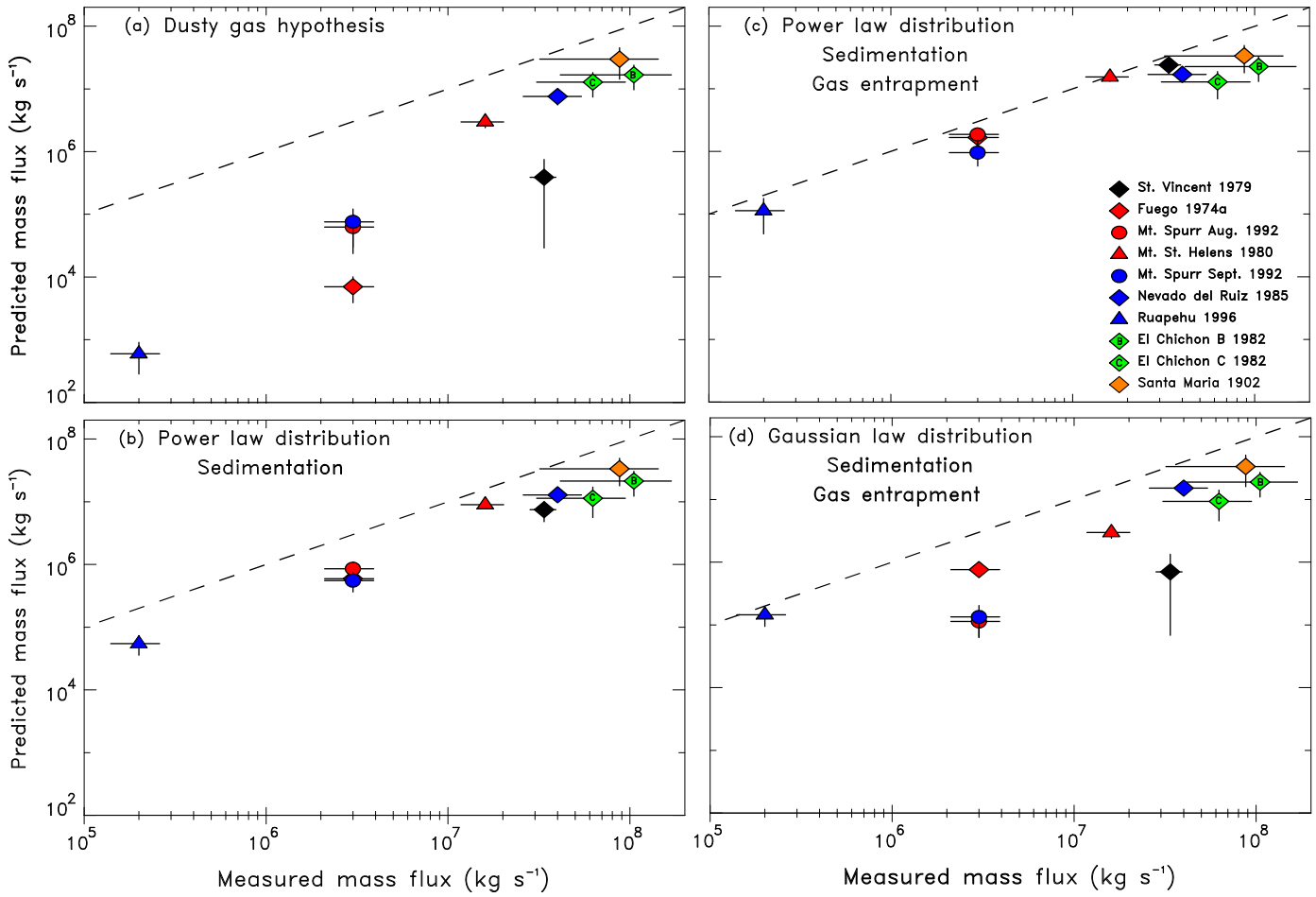

Fig. 6. Predictions of the eruptive mass flux for ten Plinian eruptions of the XXth century versus the measured eruptive mass flux. Calculations are made using four approaches: (a) classical prediction using the 'dusty gas hypothesis' (no sedimentation), (b) power-law GSD at the vent with particle sedimentation, (c) power-law GSD at the vent with particle sedimentation and gas entrapment, and (d) Gaussian-law GSD at the vent with particle sedimentation and gas entrapment. See Table 1 for the characteristics of the power laws (D) and the Gaussian laws ($\mu \pm \sigma$), and Table 2 for data of the eruptive mass fluxes.

5.3. Associated effects of wind and GSD

The mass fluxes of some eruptions, i.e., Mt. Spurr (Sept. 1992), Nevado del Ruiz (1985) and El Chichón (B + C, 1982), while better predicted using power-law GSD at the vent with the effects of particle sedimentation and gas entrapment, are still underestimated with the present model (Fig. 6c). Additional factors not included in our model and known to reduce the height of the column, such as atmospheric wind (e.g., Degruyter and Bonadonna, 2013) or thermal disequilibrium between gas and particles (e.g., Woods and Bursik, 1991) may explain the underestimated mass fluxes obtained for these eruptions. Atmospheric wind in particular may also lower the maximum height of weak plumes (i.e., mass flux smaller than 10^7 kg s^{-1}) (Woodhouse et al., 2013).

One way to estimate the influence of wind on the predicted mass fluxes is to use the analytical expression given by Degruyter and Bonadonna (2012). According to their formula, the relative difference between our prediction of mass fluxes and the same prediction in the presence of wind can be written as:

$$\frac{\Delta Q_0}{Q_0} = \left(\frac{\beta}{\alpha_e}\right)^2 \frac{z_1^4}{6 \times 2^{5/2}} \frac{\bar{v}}{\bar{N} H} - 1 = \frac{1 - \Pi}{\Pi}, \qquad (12)$$

where $z_1 = 2.8$ is the maximum non-dimensional height of Morton et al. (1956), $\bar{N} = 1.065 \times 10^{-2}$ s^{-1} is the buoyancy frequency taken as constant here as a first-order approximation and Π is a dimensionless number quantifying the effect of wind (Degruyter and Bonadonna, 2012). Using a classical value of 0.5 for the entrainment coefficient due to wind, β (e.g., Degruyter and Bonadonna, 2013), and a mean wind velocity $\bar{v}$ of 30 m s^{-1}, which generally appears to be the maximum mean value measured at some sites (e.g., Bonadonna et al., 2005), we calculate the effect of a cross-wind on the predicted mass fluxes for the ten recent Plinian eruptions studied (Fig. 8). Such a high wind velocity increases significantly the predicted mass flux of all eruptions, and the smaller the value of the maximum height, the larger the increase of the predicted mass flux. The effect of a cross-wind might therefore account for the underestimation of mass fluxes of some eruptions of our "wind-free" model. Nevertheless, a mean wind velocity of 30 m s^{-1} is too high to be applicable to all eruptions. Furthermore, a constant cross-wind profile tends also to overestimate the effect of wind relative to a real atmospheric wind profile (Bursik, 2001), hence the calculated values of mass fluxes under windy conditions correspond to an upper limit in Fig. 8.

One should also note that the effect of cross-wind is strongly controlled by the value of the entrainment coefficient due to wind, the exact value of which is poorly constrained in the literature and can vary between 0.3 to 1.0 (e.g., Bursik, 2001; Woodhouse et al., 2013; Degruyter and Bonadonna, 2013). Hence although the qualitative effect of wind is well established, a quantitative estimate still requires more stringent constraints on the evolution of turbulent entrainment in the presence of wind. Because both GSD and wind contribute to the improvement of the model predictions, we suggest that they should be studied together to better understand

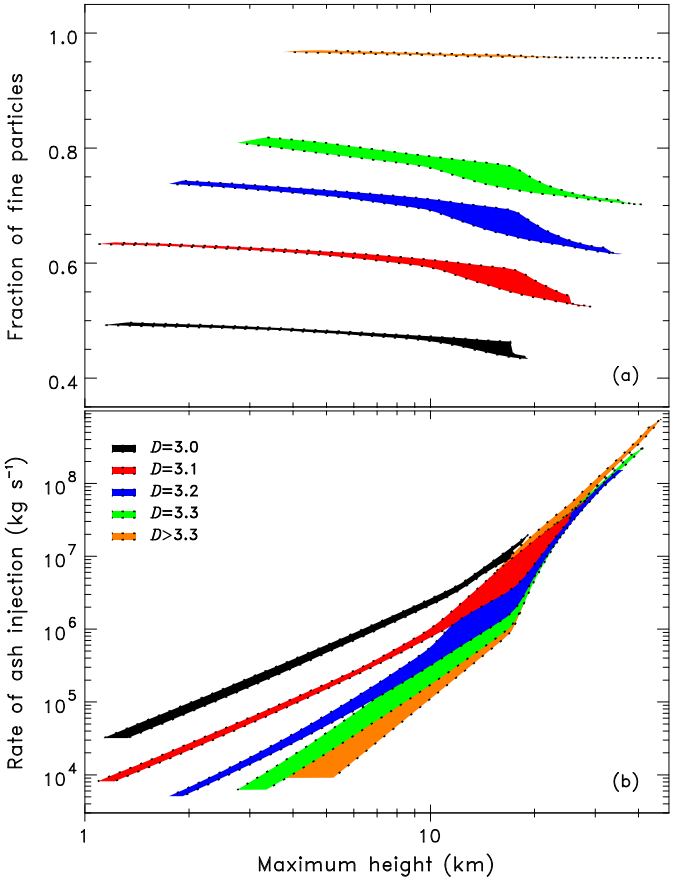

Fig. 7. Fraction of fine particles (a) and rate of ash injection into the atmosphere (b) versus maximum height reached by the column for different power-law exponents D. Colored spans represent the min–max range depending on atmospheric conditions.

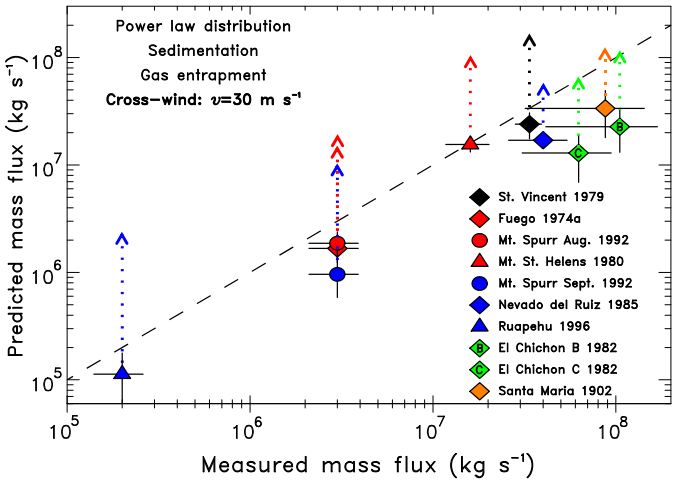

Fig. 8. Effect of a cross-wind on the predictions of the eruptive mass flux for ten Plinian eruptions of the XXth century. Vertical arrows correspond to the range of predicted mass fluxes when $v \leqslant 30\ \mathrm{m\,s^{-1}}$.

their combined influence on the column height and on the ash injection rate as a function of the eruptive mass flux.

6. Conclusion

We have shown that the power-law GSD at the vent can play a major role in the dynamics of eruptive columns. The incorporation of "real" GSD may reduce significantly the maximum height of eruptive columns, by 30 to 85% depending on the source mass flux. When the effects of particle sedimentation and gas entrapment are taken into account together with a power-law GSD at the vent, consistent with the characteristics of field deposits, we are able to better explain the measured mass flux of various Plinian eruptions than when using a classical model relying on a "dusty gas" hypothesis.

Total GSD, determined by the study of tephra deposits, combined with the modelling of turbulent processes in the volcanic plume (air entrainment and particle sedimentation) demonstrates that GSD at the neutral buoyancy and maximum heights cannot be described by a log-normal distribution as is commonly assumed. The use of log-normal GSD in modelling and satellite observation thus will lead to significant errors in the estimate of ash flow rate in the umbrella and of particle concentration in the eruptive cloud. This is an important concern when dealing with ash loading determination for risk assessment purposes. Our model is a first step toward improved and more robust predictions. Future developments should focus on the effect of atmospheric wind (Degruyter and Bonadonna, 2013), thermal disequilibrium between gas and particles (Woods and Bursik, 1991), which both reduce the height of the column for given mass flux and are likely to affect the rate of ash injection into the atmosphere, and on the effect of particle re-entrainment in the volcanic column (Ernst et al., 1996). From that point, particle aggregation and dispersion processes could also be implemented in the umbrella cloud (e.g., Textor et al., 2006; Costa et al., 2010; Telling et al., 2013).

The value of the power-law exponent, which characterizes the GSD, can be assessed from field deposits for long lasting eruptive events. However, real-time determinations would be more useful. The various satellites used by the European Volcano Observatory Space Services (EVOSS) under the SysteM for volcanic ASH plume monitoring and prediction (SMASH) project are now able to give average values of particle size at maximum height with one measurement per 15 min. This significant improvement, associated with the predictive model presented here, paves the way towards a comprehensive alert algorithm taking into account the GSD of any eruption.

Acknowledgements

This work was supported by the European Volcano Observatory Space Services (EVOSS) under the SysteM for volcanic ASH plume monitoring and prediction (SMASH) project (grant agreement 242535). The present manuscript has been improved thanks to the constructive comments of two anonymous reviewers. This is IPGP contribution number 3511.

References

Alibidirov, M., Dingwell, D.B., 1996. Magma fragmentation by rapid decompression. Nature 380, 146–148.
Anderson, E.T., 1908. The volcanoes of Guatemala. Geogr. J. 31, 473–489.
Anderson, T., Flett, J.S., 1903. Report on the eruption of the Soufrière in St. Vincent in 1902. Philos. Trans. R. Soc. Lond. A 22, 354–553.
Barnett, W.P., Kurszlaukis, S., Tait, M., Dirks, P., 2011. Kimberlite wall–rock fragmentation processes: Venetia K08 pipe development. Bull. Volcanol. 73, 941–958.
Barsotti, S., Neri, A., Scire, J.S., 2008. The VOL-CALPUFF model for atmospheric ash dispersal: 1. Approach and physical formulation. J. Geophys. Res. 113, B03208.
Baxter, P.J., Boyle, R., Cole, P., Neri, A., Spence, R., Zuccaro, G., 2005. The impacts of pyroclastic surges on buildings at the eruption of the Soufrière Hills volcano, Montserrat. Bull. Volcanol. 67, 292–313.
Bonadonna, C., Houghton, B.F., 2005. Total grain-size distribution and volume of tephra-fall deposits. Bull. Volcanol. 67, 441–456.
Bonadonna, C., Ernst, G.G.J., Sparks, R.S.J., 1998. Thickness variations and volume estimates of tephra fall deposits: the importance of particle Reynolds number. J. Volcanol. Geotherm. Res. 81, 173–187.
Bonadonna, C., Phillips, J.C., Houghton, B.F., 2005. Modeling tephra sedimentation from a Ruapehu weak plume eruption. J. Geophys. Res. 110, B08209.

Bonadonna, C., Folch, A., Loughlin, S., Puempel, H., 2012. Future developments in modelling and monitoring of volcanic ash clouds: outcomes from the first IAVCEI-WMO workshop on Ash Dispersal Forecast and Civil Aviation. Bull. Volcanol. 74, 1–10.
Brazier, S., Davis, A.N., Sigurdsson, H., Sparks, R.S.J., 1982. Fall-out and deposition of volcanic ash during the 1979 explosive eruption of the Soufrière of Saint Vincent. J. Volcanol. Geotherm. Res. 14, 335–359.
Briggs, G.A., 1969. Optimum formulas for buoyant plume rise. Philos. Trans. R. Soc. Lond. 265, 197–203.
Burden, R.E., Phillips, J.C., Hincks, T.K., 2011. Estimating volcanic plume heights from depositional clast size. J. Geophys. Res. 116, B11206.
Bursik, M., 2001. Effect of wind on the rise height of volcanic plumes. Geophys. Res. Lett. 28, 3621–3624.
Bursik, M., Carey, S., Sparks, R.S.J., Gilbert, J., 1992. Sedimentation of tephra by volcanic plumes: I. Theory and its comparison with a study of the Fogo A Plinian deposit, Sao Miguel (Azores). Bull. Volcanol. 54, 329–334.
Carazzo, G., Kaminski, E., Tait, S., 2006. The route to self-similarity in turbulent jets and plumes. J. Fluid Mech. 547, 137–148.
Carazzo, G., Kaminski, E., Tait, S., 2008a. On the rise of turbulent plumes: Quantitative effects of variable entrainment for submarine hydrothermal vents, terrestrial and extra terrestrial explosive volcanism. J. Geophys. Res. 113, B09201.
Carazzo, G., Kaminski, E., Tait, S., 2008b. On the dynamics of volcanic columns: a comparison of field data with a new model of negatively buoyant jets. J. Volcanol. Geotherm. Res. 178, 94–103.
Carazzo, G., Kaminski, E., Tait, S., 2010. The rise and fall of turbulent fountains: a new model for improved quantitative predictions. J. Fluid Mech. 657, 265–284.
Carey, S.N., Sigurdsson, H., 1978. Deep-sea evidence for distribution of tephra from mixed magma eruption of Soufrière on St-Vincent, 1902 – Ash turbidites and air fall. Geology 6, 271–274.
Carey, S., Sigurdsson, H., 1982. Influence of particle aggregation on deposition of distal tephra from May 1980 eruption of Mount St. Helens volcano. J. Geophys. Res. 87, 7061–7072.
Carey, S., Sigurdsson, H., 1986. The 1982 eruptions of El Chichon volcano, Mexico (2): Observations and numerical modelling of tephra-fall distribution. Bull. Volcanol. 48, 127–141.
Carey, S., Sigurdsson, H., 1989. The intensity of Plinian eruptions. Bull. Volcanol. 51, 28–40.
Carey, S.N., Sparks, R.S.J., 1986. Quantitative models of fallout and dispersal of tephra from volcanic eruption columns. Bull. Volcanol. 48, 109–125.
Carey, S., Sigurdsson, H., Gardner, J.E., Criswell, W., 1990. Variations in column height and magma discharge during the May 18, 1980 eruption of Mount St. Helens. J. Volcanol. Geotherm. Res. 43, 99–112.
Costa, A., Macedonio, G., Folch, A., 2006. A three-dimensional Eulerian model for transport and deposition of volcanic ashes. Earth Planet. Sci. Lett. 241, 634–647.
Costa, A., Folch, A., Macedonio, G., 2010. A model for wet aggregation of ash particles in volcanic plumes and clouds: 1. Theoretical formulation. J. Geophys. Res. 115, B09201.
Degruyter, W., Bonadonna, C., 2012. Improving on mass flow rate estimates of volcanic eruptions. Geophys. Res. Lett. 39, L16308.
Degruyter, W., Bonadonna, C., 2013. Impact of wind on the condition for column collapse of volcanic plumes. Earth Planet. Sci. Lett. 377–378, 218–226.
Dufek, J., Manga, M., Patel, A., 2012. Granular disruption during explosive volcanic eruptions. Nat. Geosci. 5, 561–564.
Durant, A.J., Rose, W.I., 2009. Sedimentological constraints on hydrometeor-enhanced particle deposition: 1992 eruptions of Crater Peak, Alaska. J. Volcanol. Geotherm. Res. 186, 40–59.
Durant, A.J., Rose, W.I., Sarna-Wojcicki, A.M., Carey, S., Volentik, A.C.M., 2009. Hydrometeor-enhanced tephra sedimentation: constraints from the 18 May 1980 eruption of Mount St. Helens. J. Geophys. Res. 114, B03204.
Eichelberger, J.C., Keith, T.E.C., Miller, T.P., Nye, C.J., 1995. The 1992 eruptions of Crater Peak vent, Mount Spurr Volcano, Alaska: Chronology and summary. In: Keith, T.E.C.E. (Ed.), The 1992 Eruptions of Crater Peak Vent, Mount Spurr Volcano, Alaska. In: U.S. Geol. Surv. Bull., vol. 2139. U.S. Government Printing Office, Washington, D.C., pp. 1–18.
Ernst, G.G.J., Sparks, R.S.J., Carey, S.N., Bursik, M.I., 1996. Sedimentation from turbulent jets and plumes. J. Geophys. Res. 101, 5575–5589.
Folch, A., Felpeto, A., 2005. A coupled model for dispersal of tephra during sustained explosive eruptions. J. Volcanol. Geotherm. Res. 145, 337–349.
Gilbert, J.S., Lane, S.J., 1994. The origin of accretionary lapilli. Bull. Volcanol. 56, 398–411.
Glaze, L.S., Baloga, S.M., 1996. Sensitivity of buoyant plume heights to ambient atmospheric conditions: Implications for volcanic eruption columns. J. Geophys. Res. 101, 1529–1540.
Glaze, L.S., Baloga, S.M., Wilson, L., 1997. Transport of atmospheric water vapor by volcanic eruption columns. J. Geophys. Res. 102, 6099–6108.
Hartmann, W.K., 1969. Terrestrial, lunar and interplanetary rock fragmentation. Icarus 10, 201–213.
Haug, Ø.T., Galland, O., Gisler, G.R., 2013. Experimental modelling of fragmentation applied to volcanic explosions. Earth Planet. Sci. Lett. 384, 188–197.
Hornwell, C.J., 2007. Grain-size analysis of volcanic ash for the rapid assessment of respiratory health hazard. J. Environ. Monit. 9, 1107–1115.
Kaminski, E., Jaupart, C., 1998. The size distribution of pyroclasts and the fragmentation sequence in explosive volcanic eruptions. J. Geophys. Res. 103, 29759–29779.
Kaminski, E., Jaupart, C., 2001. Marginal stability of atmospheric eruption columns and pyroclastic flow generation. J. Geophys. Res. 106, 21785–21798.
Kaminski, E., Tait, S., Carazzo, G., 2005. Turbulent entrainment in jets with arbitrary buoyancy. J. Fluid Mech. 526, 361–376.
Kaminski, E., Tait, S., Ferrucci, F., Martet, M., Hirn, B., Husson, P., 2011. Estimation of ash injection in the atmosphere by basaltic volcanic plumes: The case of the Eyjafjallajökull 2010 eruption. J. Geophys. Res. 116, B00C02.
Koyaguchi, T., Ohno, M., 2001. Reconstruction of eruption column dynamics on the basis of grain size of tephra fall deposits 1. Methods. J. Geophys. Res. 106, 6499–6512.
Koyaguchi, T., Suzuki, Y.J., Kozono, T., 2010. Effects of the crater on eruption column dynamics. J. Geophys. Res. 115, B07205.
Kueppers, U., Perugini, D., Dingwell, D.B., 2006. "Explosive energy" during volcanic eruptions from fractal analysis of pyroclasts. Earth Planet. Sci. Lett. 248, 800–807.
Mastin, L.G., 2007. A user-friendly one-dimensional model for wet volcanic plumes. Geochem. Geophys. Geosyst. 8, Q03014.
Mastin, L.G., Guffanti, M., Servranckx, R., Webley, P., Barsotti, S., Dean, K., Durant, A., Ewert, J.W., Neri, A., Rose, W.I., Schneider, D., Siebert, L., Stunder, B., Swanson, G., Tupper, A., Volentik, A., Waythomas, C.F., 2009. A multidisciplinary effort to assign realistic source parameters to models of volcanic ash-cloud transport and dispersion during eruptions. J. Volcanol. Geotherm. Res. 186, 10–21.
McGimsey, R.G., Neal, C.A., Riley, C., 2001. Areal distribution, thickness, volume, and grain size of tephra-fall deposits from the 1992 eruptions of Crater Peak vent, Mt. Spurr volcano, Alaska. U.S. Geological Survey Open-File Report 01-0370. U.S. Government Printing Office, Washington, D.C., 38 pp.
Miller, T.P., Casadevall, T.J., 2000. Volcanic ash hazards to aviation. In: Sigurdsson, H.E. (Ed.), Encyclopedia of Volcanoes. Academic Press, San Diego, pp. 915–930.
Morton, B.R., Taylor, G.I., Turner, J.S., 1956. Turbulent gravitational convection from maintained and instantaneous source. Proc. R. Soc. Lond. 234, 1–23.
Murrow, P.J., Rose Jr., W.I., Self, S., 1980. Determination of the total grain size distribution in a Vulcanian eruption column, and its implications to stratospheric aerosol perturbation. Geophys. Res. Lett. 7, 893–896.
Naranjo, J.L., Sigurdsson, H., Carey, S.N., Fritz, W., 1986. Eruption of the Nevado del Ruiz volcano, Colombia, on 13 November 1985: tephra fall and lahars. Science 233, 961–963.
Neal, C.A., McGimsey, R.G., Gardner, C.A., Harbin, M.L., Nye, C.J., 1995. Tephra-fall deposits from the 1992 eruptions of Crater Peak, Mount Spurr Volcano, Alaska: a preliminary report on distribution, stratigraphy, and composition. In: K.T. (Ed.), The 1992 Eruptions of Crater Peak Vent, Mount Spurr Volcano, Alaska. In: U.S. Geol. Surv. Bull., pp. 65–79.
Ogden, D.E., Glatzmaier, G.A., Wohletz, K.H., 2008. Effects of vent overpressure on buoyant eruption columns: Implications for plume stability. Earth Planet. Sci. Lett. 268, 283–292.
Ongaro, T.E., Cavazzoni, C., Erbacci, G., Neri, A., Salvetti, M.V., 2007. A parallel multiphase flow code for the 3D simulation of explosive volcanic eruptions. Parallel Comput. 33, 541–560.
Pfeiffer, T., Costa, A., Macedonio, G., 2005. A model for the numerical simulation of tephra fall deposits. J. Volcanol. Geotherm. Res. 140, 273–294.
Pike, W.T., Staufer, U., Hecht, M.H., Goetz, W., Parrat, D., Sykulska-Lawrence, H., Vijendran, S., Madsen, M.B., 2011. Quantification of the dry history of the Martian soil inferred from in situ microscopy. Geophys. Res. Lett. 38, L24201.
Prata, A.J., Grant, I.F., 2001. Retrieval of microphysical and morphological properties of volcanic ash plumes from satellite data: application to Mt. Ruapehu, New Zealand. Q. J. R. Meteorol. Soc. 127, 2153–2179.
Prata, A.J., Prata, A.T., 2012. Eyjafjallajökull volcanic ash concentrations determined using Spin Enhanced Visible and Infrared Imager measurements. J. Geophys. Res. 117, D00U23.
Robock, A., 2000. Volcanic eruptions and climate. Rev. Geophys. 38, 191–219.
Rose, W.I., 1972. Notes on the 1902 eruption of Santa Maria volcano, Guatemala. Bull. Volcanol. 36, 29–45.
Rose, W.I., Durant, A.J., 2009. El Chichón volcano, April 4, 1982: volcanic cloud history and fine ash fallout. Nat. Hazards 51, 363–374.
Rose, W.I., Self, S., Murrow, P.J., Bonadonna, C., Durant, A.J., Ernst, G.G.J., 2008. Nature and significance of small volume fall deposits at composite volcanoes: insights from the October 14, 1974 Fuego eruption, Guatemala. Bull. Volcanol. 70, 1043–1067.
Sarna-Wojcicki, A.M., Shipley, S., Waitt, R.B., Dzurisin, D., Wood, S.H., 1981. Areal distribution, thickness, mass, volume and grain size of air-fall ash from the six major eruptions of 1980. In: Lipman, P.W., Mullineaux, D.R. (Eds.), The 1980 Eruptions of Mount St. Helens, Washington, pp. 577–628.
Settle, M., 1978. Volcanic eruption clouds and the thermal power output of explosive eruptions. J. Volcanol. Geotherm. Res. 3, 309–324.
Slingo, J., 2010. Society's growing vulnerability to natural hazards and implications for geophysics research. Eos Trans. AGU 91, U15A–01.
Sparks, R.S.J., 1986. The dimensions and dynamics of volcanic eruption columns. Bull. Volcanol. 48, 3–15.

Sparks, R.S.J., Wilson, L., 1982. Explosive volcanic eruptions. 5. Observations of plume dynamics during the 1979 Soufrière eruption, St. Vincent. Geophys. J. R. Astron. Soc. 69, 551–570.
Sparks, R.S.J., Bursik, M., Carey, S., Gilbert, J.S., Glaze, L.S., Sigurdsson, H., Woods, A.W., 1997. Volcanic Plumes. John Wiley, New York, 574 pp.
Suzuki, Y.J., Koyaguchi, T., 2012. 3-D numerical simulations of eruption column collapse: Effects of vent size on pressure-balanced jet/plumes. J. Volcanol. Geotherm. Res. 221–222, 1–13.
Telling, J., Dufek, J., Shaikh, A., 2013. Ash aggregation in explosive volcanic eruptions. Geophys. Res. Lett. 40, 2355–2360.
Textor, C., Graf, H.F., Herzog, M., Oberhuber, J.M., Rose, W.I., Ernst, G.G.J., 2006. Volcanic particle aggregation in explosive eruption columns. Part II: Numerical experiments. J. Volcanol. Geotherm. Res. 150, 378–394.
Turcotte, D.L., 1986. Fractals and fragmentation. J. Geophys. Res. 91, 1921–1926.
Valentine, G.A., Wohletz, K.H., 1989. Numerical models of Plinian eruption columns and pyroclastic flows. J. Geophys. Res. 94, 1867–1887.
Veitch, G., Woods, A.W., 2000. Particle recycling and oscillations of volcanic eruption columns. J. Geophys. Res. 105, 2829–2842.
Williams, S.N., Self, S., 1983. The October 1902, Plinian eruption of Santa Maria volcano, Guatemala. J. Volcanol. Geotherm. Res. 16, 33–56.
Wilson, L., 1976. Explosive volcanic eruptions: III. Plinian eruption columns. J. R. Astron. Soc. 45, 543–556.
Wilson, L., Sparks, R.S.J., Huang, T.C., Watkins, N.D., 1978. The control of volcanic column heights by eruption energetics and dynamics. J. Geophys. Res. 83, 1829–1836.
Woodhouse, M.J., Hogg, A.J., Phillips, J.C., Sparks, R.S.J., 2013. Interaction between volcanic plumes and wind during the 2010 Eyjafjallajökull eruption, Iceland. J. Geophys. Res., Solid Earth 118. http://dx.doi.org/10.1029/2012JB009592.
Woods, A.W., 1988. The fluid dynamics and thermodynamics of eruption columns. Bull. Volcanol. 50, 169–193.
Woods, A.W., 1993. Moist convection and the injection of volcanic ash into the atmosphere. J. Geophys. Res. 98, 17627–17636.
Woods, A.W., Bower, S.M., 1995. The decompression of volcanic jets in a crater during explosive volcanic eruptions. Earth Planet. Sci. Lett. 131, 189–205.
Woods, A.W., Bursik, M.I., 1991. Particle fallout, thermal disequilibrium and volcanic plumes. Bull. Volcanol. 53, 559–570.